Familial hemiplegic migraine mutations increase Ca^{2+} influx through single human $Ca_V2.1$ channels and decrease maximal $Ca_V2.1$ current density in neurons

Angelita Tottene*†, Tommaso Fellin*†, Stefano Pagnutti*, Siro Luvisetto*, Joerg Striessnig‡, Colin Fletcher§, and Daniela Pietrobon*¶

*Department of Biomedical Sciences, University of Padova, 35121 Padova, Italy; ‡Department of Pharmacology and Toxicology, Institute of Pharmacy, University of Innsbruck, A-6020 Innsbruck, Austria; and §Genomics Institute of the Novartis Research Foundation and Department of Cell Biology, The Scripps Research Institute, La Jolla, CA 92037

Edited by William A. Catterall, University of Washington School of Medicine, Seattle, WA, and approved July 29, 2002 (received for review April 23, 2002)

Insights into the pathogenesis of migraine with aura may be gained from a study of human $Ca_V2.1$ channels containing mutations linked to familial hemiplegic migraine (FHM). Here, we extend the previous single-channel analysis to human $Ca_V2.1$ channels containing mutation V1457L. This mutation increased the channel open probability by shifting its activation to more negative voltages and reduced both the unitary conductance and the density of functional channels in the membrane. To investigate the possibility of changes in $Ca_V2.1$ function common to all FHM mutations, we calculated the product of single-channel current and open probability as a measure of Ca^{2+} influx through single $Ca_V2.1$ channels. All five FHM mutants analyzed showed a single-channel Ca^{2+} influx larger than wild type in a broad voltage range around the threshold of activation. We also expressed the FHM mutants in cerebellar granule cells from $Ca_V2.1\alpha_1^{-/-}$ mice rather than HEK293 cells. The FHM mutations invariably led to a decrease of the maximal $Ca_V2.1$ current density in neurons. Current densities were similar to wild type at lower voltages because of the negatively shifted activation of FHM mutants. Our data show that mutational changes of functional channel densities can be different in different cell types, and they uncover two functional effects common to all FHM mutations analyzed: increase of single-channel Ca^{2+} influx and decrease of maximal $Ca_V2.1$ current density in neurons. We discuss the relevance of these findings for the pathogenesis of migraine with aura.

Migraine is a debilitating illness, characterized by attacks of severe, unilateral headache, which afflicts 10–15% of the population. Attacks can be preceded by an "aura," most frequently consisting of scintillations that slowly drift across the visual field. Functional brain imaging and magnetoencephalography in patients (1, 2) have provided evidence that the visual aura is the result of cortical spreading depression (CSD), a wave of neuronal depolarization that spreads slowly across the cerebral cortex (3, 4). Evidence from both animal models and humans indicates that the headache is a consequence of activation of trigeminovascular afferents innervating the meninges, causing neurogenic inflammation and activation of trigeminal nucleus caudalis and brainstem nuclei involved in the perception of pain (5, 6). Recently, Bolay *et al.* (7) have shown that CSD in the rat cortex activates trigeminovascular afferents and evokes a series of alterations in the meninges and brainstem consistent with the development of headache. These data, together with earlier work, point to CSD as the critical event in the pathogenesis of migraine with aura, but it remains unknown what would make the brain of patients more susceptible to CSD.

Insights may be gained from the study of familial hemiplegic migraine (FHM), a dominantly inherited subtype of migraine with aura associated with ictal hemiparesis. In half of the families tested, FHM is caused by missense mutations in CACNA1A (8), the gene encoding the pore-forming α_1-subunit of $Ca_V2.1$ (voltage-gated P/Q-type Ca^{2+}) channels (9–12). $Ca_V2.1$ channels are located in presynaptic terminals throughout the brain (13) and play a prominent role in controlling neurotransmitter release at most synapses (14). Their localization in somatodendritic membranes points to additional postsynaptic roles (15–17). Studies of mutant $Ca_V2.1$ channels in heterologous expression systems revealed that FHM mutations alter both the single-channel biophysical properties and the density of functional channels in the membrane (18–20). Alterations in single-channel function included an almost general increase in open probability, a reduction in conductance (by some FHM mutations), and variable effects on channel inactivation. The density of functional channels in the membrane was reduced by most mutations but was increased by one mutation. Overall, the changes induced by the FHM mutations led to the prediction of a decreased or increased whole-cell Ca^{2+} influx, depending on the mutation (18).

To investigate the possibility of changes in $Ca_V2.1$ function common to all FHM mutations, we calculated the product of single-channel current and open probability as a measure of the Ca^{2+} influx through single human $Ca_V2.1$ channels and extended the previous single-channel analysis to mutation V1457L (20). We also expressed FHM mutants in $Ca_V2.1$-deficient neurons rather than HEK293 cells. We uncovered two common changes in $Ca_V2.1$ function caused by FHM mutations: an increased single-channel Ca^{2+} influx and a decreased maximal $Ca_V2.1$ current density in neurons, and discuss their relevance for the pathogenesis of migraine with aura.

Methods

Cell Culture and Transfection. HEK293 cells were grown and cotransfected with human $Ca_V2.1\alpha_1$ ($\alpha_{1A\text{-}2}$), β_{2e}, and $\alpha_{2b}\delta$ cDNAs, as described (18). The constructs encoding mutants T666M, V714A, I1815L, and R192Q were those described in (18). Mutation V1457L was introduced into the human $Ca_V2.1\alpha_1$ cDNA described in ref. 21 and differs from $\alpha_{1A\text{-}2}$ by one splice deletion ($V^{726}EA$). To construct the mutant clone V1457L, fusion PCR was applied to generate an *Eco*RI–*Kpn*I (nucleotides 4319–4450) fragment carrying a G-to-C (nucleotide 4366) substitution. This PCR fragment was added to an *Aat*II–*Eco*RI

This paper was submitted directly (Track II) to the PNAS office.

Abbreviations: CSD, cortical spreading depression; FHM, familial hemiplegic migraine; I-V, current–voltage relationship; wt, wild type; TEA, tetraethylammonium.

†A.T. and T.F. contributed equally to this work.

¶To whom reprint requests should be addressed at: Department of Biomedical Sciences, University of Padova, Viale G. Colombo 3, 35121 Padova, Italy. E-mail: dani@civ.bio.unipd.it.

 www.pnas.org/cgi/doi/10.1073/pnas.192242399

(nucleotides 2875–4319) subclone of $Ca_V2.1\alpha_1$ inserted in pSport-1 (Invitrogen). Finally, the *Spl*I–*Kpn*I (nucleotides 3039–4450) fragment of this new subclone was ligated into the corresponding sites of $Ca_V2.1\alpha_1$ in $pGFP^-$ (21). Cells transfected with $\alpha_{1A\text{-}2}$ were incubated at 28°C for 14–20 h before recording, because this procedure increased expression (18). Incubation at 28°C was not necessary for cells transfected with $\alpha_{1A\text{-}2}$(-VEA), given the higher expression level. Identical normalized whole-cell current-voltage (I-V) relationships, and also identical single-channel current, i, and open probability, po, as a function of voltage, were measured in cells expressing the $\alpha_{1A\text{-}2}$ and $\alpha_{1A\text{-}2}$(-VEA) subunits. The data were then pooled together.

Cerebellar granule cells were grown in primary culture from 6-day-old $Ca_V2.1\alpha_1^{-/-}$ mice as described (12). Experiments were performed on cells grown from 5 to 7 days *in vitro*. Cells were transfected with wild-type (wt) or mutant human $\alpha_{1A\text{-}2}$ cDNA at day 2 by using the modified calcium phosphate procedure described in ref. 22, except for a higher concentration of DNA per plate (for each 35-mm diameter plate, 4 and 8 μg for the reporter GFP and the α_1-subunit, respectively), and for the absence of ionotropic glutamate receptor inhibitors in the transfection medium (Eagle's minimal essential medium with Hanks' salts/25 mM Hepes, pH 7.85). Typically, the incubation with the DNA/calcium phosphate precipitate was stopped 15 min after precipitate was formed.

Patch-Clamp Recordings and Data Analysis. Whole-cell patch-clamp recordings were performed as in ref. 12 and single-channel recordings as in ref. 18. Currents were sampled at 5 kHz and low-pass filtered at 1 kHz.

External solution for whole-cell recordings was 5 mM $BaCl_2$ (or $CaCl_2$), 148 mM tetraethylammonium (TEA)-Cl, 10 mM Hepes (pH 7.4 with TEA-OH) (and 5 μM nimodipine and 0.1 mg/ml cytochrome C, when recording from neurons). Internal solution was 100 mM Cs-methanesulfonate/5 mM $MgCl_2$/30 mM Hepes/10 mM EGTA/4 mM ATP/0.5 mM GTP/1 mM c-AMP (pH 7.4 with CsOH). Compensation (typically 70–80%) for series resistance was used, and I-V curves were obtained only from cells with a voltage error <5 mV. The average normalized I-V curves were multiplied by the average maximal current density obtained from all cells. I-V curves in HEK cells were obtained with voltage ramps (0.85 mV/msec) from a holding potential of −80 mV. I-V ramps for leak subtraction were obtained after blockade of Ca^{2+} channels with 5–10 mM Ni^{2+}. I-V curves were fitted with Eq. **1**:

$$I = G(V - E_{rev})\{1 + \exp[(V_{1/2} - V)/k]\}^{-1}. \quad [1]$$

Single-channel recordings were obtained in cell-attached configuration. Pipette solution was 90 mM $BaCl_2$/10 mM TEA-Cl/15 mM CsCl/10 mM Hepes or 10 mM $BaCl_2$ (or $CaCl_2$)/130 mM TEA-Cl/15 mM CsCl/10 mM Hepes (pH 7.4 with TEA-OH). Bath solution was 140 mM K-gluconate/5 mM EGTA/35 mM L-glucose/10 mM Hepes (pH 7.4 with KOH). Quartz pipettes were used with 10 mM Ca^{2+} as charge carriers. Single-channel currents and open probabilities were obtained as in ref. 18.

The density of functional channels in the membrane for mutant V1457L relative to that of wt channels was obtained from Eq. **2**:

$$N_{mt}/N_{wt} = (I_{mt}/I_{wt})/(i_{mt}po_{mt}/i_{wt}po_{wt}), \quad [2]$$

with the current densities, I_{mt} and I_{wt}, and the products of single-channel current and open probability, $i_{mt}po_{mt}$ and $i_{wt}po_{wt}$, measured at the peak of the I-V and ipo-V curves obtained for mutant and wt channels, respectively.

In both whole-cell (12) and single-channel recordings (90 mM Ba^{2+}), the liquid junction potentials were such that a value of 12 mV should be subtracted from all voltages to obtain the correct values of membrane potential. Averages are given ± SEM.

Results

Human $\alpha_{1A\text{-}2}$-subunits containing the five different mutations linked to FHM shown in Fig. 1 were coexpressed with human $\alpha_{2b}\delta$- and β_{2e}-subunits in HEK293 cells. Fig. 1*A* shows the relative whole-cell Ba^{2+} current densities measured as a function of voltage in cells expressing wt channels (wt) or $Ca_V2.1$ mutants containing mutations T666M (TM) and V1457L (VL), located close to glutamate residues forming the high-affinity binding site for Ca^{2+} ions in the pore. Near the threshold of activation, the current density of the VL mutant was similar to wt, whereas it was much smaller at higher voltages. Single-channel recordings revealed that a decreased single-channel current, i, and conductance (from 19.6 ± 0.2 pS, n = 19 to 12.6 ± 0.2 pS, n = 11) contribute to the smaller current density; on the other hand, a shift to more negative voltages of the voltage-dependence of the channel open probability, po, accounts for the current density similar to wt at low voltages (Fig. 1*A*). Given the similar maximal po of wt and VL channels and the less than 50% decreased unitary conductance of VL, a reduction of the density of functional channels in the membrane must contribute to the almost 70% decrease of the maximal whole-cell current density of the mutant. The estimated density of functional mutant channels with respect to wt channels was 0.45 ± 0.10 (from Eq. **2** in *Methods*). As reported for human $Ca_V2.1$ channels containing the β_{3a}-subunit (18), the whole-cell current density of the TM mutant was smaller than wt at all voltages, as a consequence of an even smaller unitary current and conductance and lower density of functional channels in the membrane than VL (18). For both pore mutants the reversal potential, E_{rev}, of the Ba^{2+} current was 15 mV smaller than for wt, indicating that both mutations decrease the selectivity of the channel for Ca^{2+} with respect to monovalent ions (compare similar effect on E_{rev} with Ca^{2+} as charge carrier; Fig. 2).

If one considers the macroscopic current densities in Fig. 1 and those obtained by Hans *et al.* (18) for mutations V714A (VA), I1815L (IL), and R192Q (RQ), one would not be able to predict a common functional effect of FHM mutations on Ca^{2+} influx. In fact, the Ba^{2+} current density may be larger or smaller than wt at any voltage, depending on the mutation. Nor can one find a common denominator among the different mutations if one considers their effect on inactivation properties (18–20). On the other hand, because a common property of FHM mutants seems to be an increased po over a broad voltage range (Fig. 1*A* and ref. 18), we wondered whether, despite the decreased unitary conductance of VL (Fig. 1*A*) and of both TM and VA mutants (18), a common functional effect of the FHM mutations was an increased single-channel Ca^{2+} influx, as given by the product of single-channel current and open probability, ipo.

Fig. 1*B* shows the ipo values calculated as a function of voltage for the wt and the five mutant channels. Indeed, at low voltages, around the threshold of activation, the single-channel Ba^{2+} influx, as measured by the product ipo, was larger than wt for all FHM mutants. Thus, even for the two pore mutants (TM and VL) with considerably reduced single-channel conductance, the shift of channel activation to more negative voltages produces an increase in po that is more than sufficient to compensate for the reduction in unitary current over a broad voltage range. Moreover, all FHM mutants exhibit a significant single-channel Ba^{2+} influx at voltages where the open probability of wt channels is insignificant. For VA mutants, similar ipo values were obtained for the prevalent mutants with reduced conductance and for the minority of mutants with wt conductance, given the lower po of the latter (ref. 18, and data not shown).

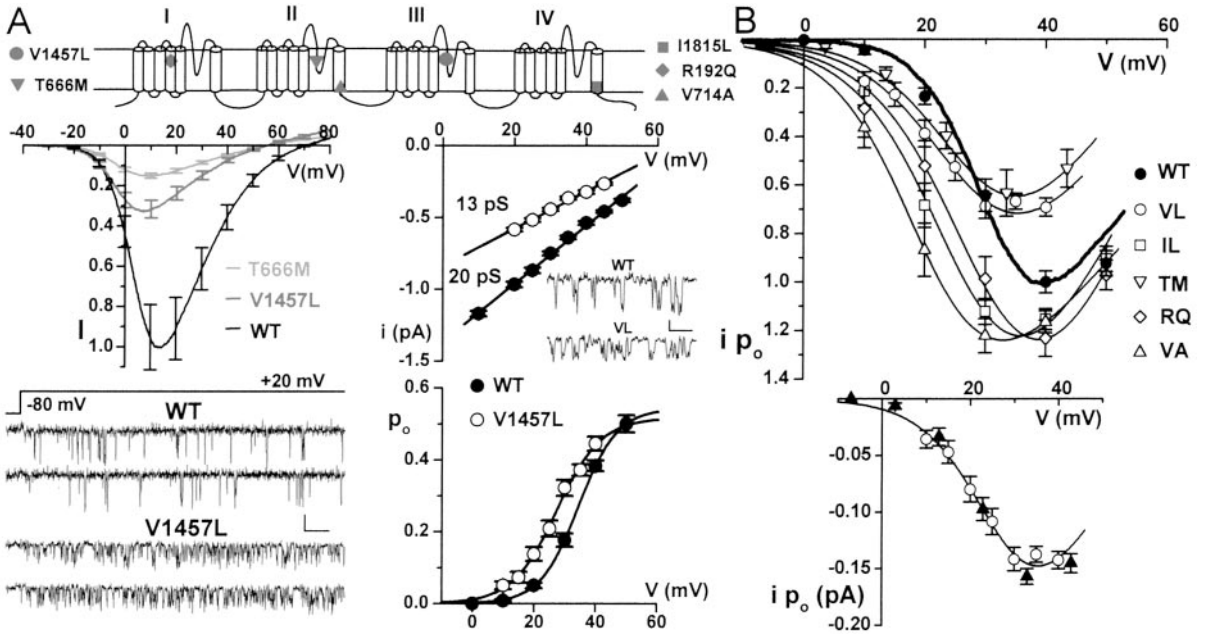

Fig. 1. FHM mutations increase Ba^{2+} influx through single human $Ca_V2.1$ channels. (*A Top Left*) Whole-cell recordings with 5 mM Ba^{2+} as charge carrier. Whole-cell current densities during voltage ramps were measured in HEK293 cells expressing human wt and mutant V1457L (VL) and T666M (TM) $Ca_V2.1$ channels. Maximal current densities in cells transfected with $\alpha_{1A\text{-}2}$ and $\alpha_{1A\text{-}2}$ (-VEA) cDNAs were 70.6 ± 12.0 pA/pF, n = 52, and 71.6 ± 11.3 pA/pF, n = 31, respectively. Identical normalized current density-voltage (I-V) curves were measured for the two wt isoforms (n = 9 and n = 12, respectively). Maximal current densities of the $\alpha_{1A\text{-}2}$TM and $\alpha_{1A\text{-}2}$ (-VEA) VL mutants were 10.7 ± 0.9 pA/pF (n = 53) and 22.7 ± 3.1 pA/pF (n = 32), respectively. The I-V curves of the mutants were divided by the maximal current density of the corresponding wt channels. (*A Bottom Left*) Single-channel cell-attached recordings on HEK cells expressing wt and mutant VL channels; 90 mM Ba^{2+} as charge carrier. Holding potential = −80 mV. Representative current traces from single-channel patches containing a wt $Ca_V2.1$ channel (cell X24A) or a VL mutant (cell A07B). (Bars = 0.5 pA, 40 ms.) (*A Right*) Unitary current, i, and open probability, po, as a function of voltage, for wt and VL mutant channels. (*Top*) Average I-V curves from 19 (wt) and 11 (VL) patches. (*Inset*) Unitary activity at 20 mV on an expanded time scale. (Bars = 0.3 pA, 10 ms.) (*Bottom*) Average po-V curves from 12 (wt) and 10 (VL) patches containing a single channel. The data points were best fitted by Boltzmann distributions with $V_{1/2}$ = 34.5 mV (k = 6.2) for wt and $V_{1/2}$ = 27.4 mV (k = 7.2) for VL. (*B*) Single-channel cell-attached recordings (90 mM Ba^{2+}) on HEK cells expressing wt and mutant TM, VL, R192Q (RQ), V714A (VA), and I1815L (IL) $Ca_V2.1$ channels. (*Top*) Product of i and po, as a function of voltage, for the wt channel and the five FHM mutants. All ipo values were divided by the maximal ipo value of the wt channel (−0.21 ± 0.01 pA). Values of i and po for RQ, VA, and IL mutants, and i for TM, were taken from ref. 18; po values for TM were obtained as described in the text. For the wt channel, the normalized ipo values were well fitted by the normalized whole-cell I-V curve, shifted by 26 mV toward more positive voltages (thick line). This shift accounts for the difference in surface potential in the single-channel and whole-cell recording solutions (90 vs. 5 mM Ba^{2+}). (*Bottom*) Comparison of ipo values for the VL mutant, calculated by using either the po values measured in cell-attached recordings (○) or the po values derived from the wt po-V curve in Fig. 1*A*, shifted in the hyperpolarizing direction of 7.1 mV, corresponding to the difference in $V_{1/2}$ activation estimated from fitting the whole-cell current densities of wt and VL channels with Eq. **1** (▲).

Because the very small current (i = 0.3 pA at 30 mV) and fast gating of the TM mutant precluded a reliable measurement of its po as a function of voltage, the po values for TM were obtained in an indirect manner by combining single-channel and whole-cell data. The current density curves in Fig. 1*A* revealed that the TM mutant activates at more negative voltages than the wt channel, and a 6.5-mV difference in $V_{1/2}$ activation was estimated from fitting the curves with Eq. **1** in *Methods*. A po-V curve for the TM mutant was obtained by shifting 6.5 mV in the hyperpolarizing direction the po-V curve of the wt channel; the po values thus obtained were multiplied by the measured unitary current of the TM mutant at each voltage to calculate the ipo values shown in Fig. 1*B*. The validity of this method was tested by applying it to the VL mutant: Fig. 1*B Bottom* shows a very good agreement between the measured and calculated ipo values. The good agreement also implies that the effect of the mutation on channel activation is independent of permeant ion concentration. The same is true for its effect on unitary conductance, because a similar decrease was measured with 90 and 10 mM Ba^{2+} (not shown). To infer the voltage-dependence of the single-channel Ba^{2+} influx with 5 mM Ba^{2+} as charge carrier, one can then simply shift the curves in Fig. 1*B* of 26 mV in the hyperpolarizing direction to account for the larger surface potential (see Fig. 1 legend).

The data in Fig. 2 suggest that the TM mutation increases more the single-channel Ca^{2+} than Ba^{2+} influx. With Ca^{2+} (5 mM), the maximal whole-cell current of wt channels was 45 ± 2% (n = 9) smaller than with Ba^{2+} (Fig. 2*A*), mainly as a consequence of a smaller single-channel conductance. Indeed, the single-channel conductance of $Ca_V2.1$ channels was 14.7 ± 0.2 pS (n = 8) with 10 mM Ba^{2+} and 7.3 ± 0.2 pS (n = 4) with 10 mM Ca^{2+} (Fig. 2*A*). A similar decrease in conductance can be inferred from the ascending parts of the whole-cell I-V curves (fitting with Eq. **1**, gives G_{Ca}/G_{Ba} = 0.51). For the TM mutant, the maximal Ca^{2+} current was only 25 ± 1% (n = 11) smaller than the Ba^{2+} current, and the I-V fits gave G_{Ca}/G_{Ba} = 0.76 (Fig. 2*B*). This finding is consistent with the conclusion that, with respect to the wt channel, the mutant has a larger unitary conductance for Ca^{2+} relative to Ba^{2+}, and, therefore, that mutation TM decreases less the single-channel conductance for Ca^{2+} than for Ba^{2+} ions. Single-channel recordings, recently performed with 90 mM Ca^{2+} as charge carrier, confirmed this conclusion (not shown).

The single-channel Ca^{2+} influx of the TM mutant relative to that of the wt channel, with nearly physiological concentrations of Ca^{2+} ions, was estimated by combining whole-cell and single-channel recordings, as follows. The whole-cell Ca^{2+} current density of the TM mutant relative to that of the wt channel was divided by the density of functional channels in the membrane

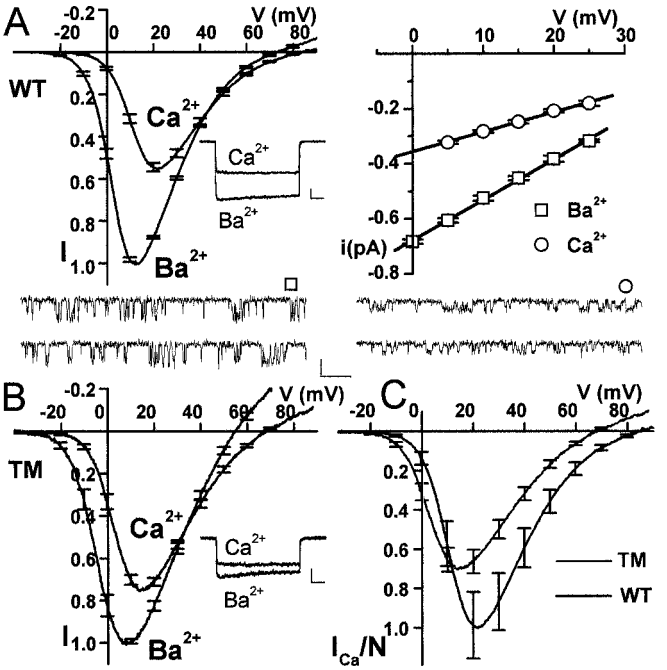

Fig. 2. The T666M mutation increases more the single-channel Ca^{2+} than the Ba^{2+} influx. (*A Left*) Whole-cell recordings with 5 mM Ba^{2+} or 5 mM Ca^{2+} as charge carriers, on HEK cells expressing wt $Ca_V2.1$ channels. Voltage ramps were applied after perfusion of each cell with Ca^{2+} and then again Ba^{2+} solution. The Ca^{2+} and Ba^{2+} current curves were normalized to the maximal value of the Ba^{2+} current in each cell ($n = 9$). (*Inset*) Representative traces of Ca^{2+} and Ba^{2+} current recorded at 20 mV (Cell S93C). (Bars = 100 pA, 20 ms.) (*A Right* and traces) Single-channel cell-attached recordings with 10 mM Ba^{2+} or 10 mM Ca^{2+} as charge carrier, from HEK cells expressing wt channels. Holding potential = −80 mV. Average I-V relationships ($n = 8$ with Ba^{2+} and $n = 4$ with Ca^{2+}; slope conductances: $g = 14.7$ and 7.2 pS) and representative current traces at 10 mV of a wt $Ca_V2.1$ channel with Ba^{2+} (*Left*, cell R43C) and Ca^{2+} (*Right*, cell R37A) as charge carrier. (Bars = 0.5 pA, 40 ms.) (*B*) Whole-cell recordings as in *A* but on cells expressing the TM mutant ($n = 11$). (*Inset*) Representative traces recorded at 10 mV (cell S85F). (Bars = 50 pA, 20 ms.) (*C*) Single-channel Ca^{2+} influx of the TM mutant relative to that of the wt channel, as a function of voltage, was estimated as follows. The whole-cell Ca^{2+} (5 mM) current density of the TM mutant relative to that of wt was divided by the density of functional TM mutants in the membrane relative to that of wt, $N_{mt}/N_{wt} = 0.31 \pm 0.03$ (obtained in two independent ways, see text). The Ca^{2+} current densities as a function of voltage were obtained by multiplying the average normalized Ca^{2+} currents recorded during voltage ramps (as in *A*) by the average peak Ca^{2+} current density of 38.8 ± 6.4 pA/pF for the wt (55 ± 2% of the Ba^{2+} current density in 52 cells) and 8.0 ± 0.7 pA/pF for TM (75 ± 1% of the Ba^{2+} current density in 53 cells).

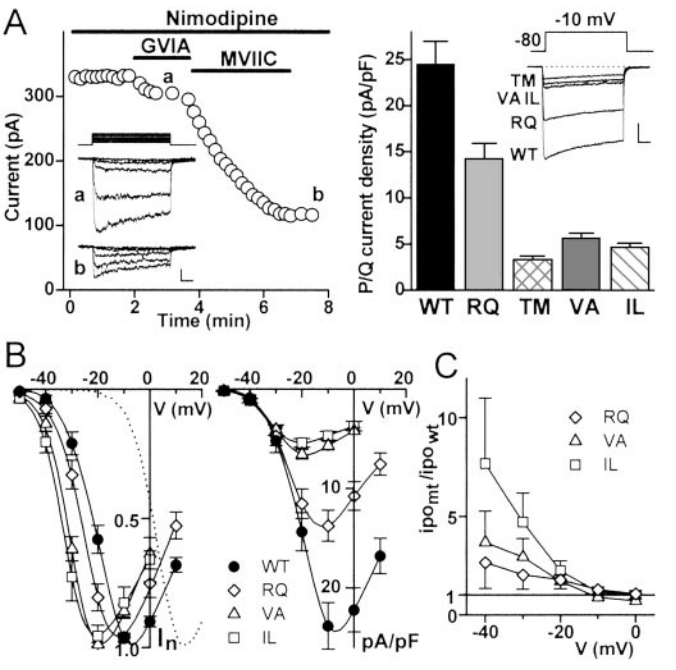

Fig. 3. Functional effects of FHM mutations in $Ca_V2.1\alpha_1^{-/-}$ neurons expressing human $Ca_V2.1\alpha_1$-subunits. Whole-cell recordings (5 mM Ba^{2+}) on cerebellar granule cells of $Ca_V2.1\alpha_1^{-/-}$ mouse transfected with wt or mutant human $Ca_V2.1\alpha_1$ ($\alpha_{1A\text{-}2}$) subunits. (*A Left*) Plot of peak current vs. time for a representative experiment on a neuron transfected with wt $\alpha_{1A\text{-}2}$-subunits (cell U280B). Depolarizations at −10 mV were delivered every 10 s from −80 mV. ω-CgTx-GVIA (1 μM) and ω-CTx-MVIIC (3 μM) were sequentially applied in the continuous presence of nimodipine (5 μM). (*Inset*) Representative traces at increasing voltages (from −50 to −10 mV) taken at times a and b. $Ca_V2.1$ currents were obtained as the difference between traces at times a and b. (Bars = 20 ms, 50 pA.) (*A Right*) Average density of $Ca_V2.1$ current at −10 mV in neurons transfected with the wt human $\alpha_{1A\text{-}2}$-subunit ($n = 32$) or the RQ ($n = 22$), TM ($n = 19$), VA ($n = 14$), and IL ($n = 12$) mutants, from 7, 5, 3, 2, and 4 neuronal cultures, respectively. (*Inset*) Corresponding pooled $Ca_V2.1$ current traces ($n =$ 10 for wt, $n = 10$ RQ, $n = 8$ TM, $n = 6$ VA, $n = 6$ IL). (Bars = 20 ms, 5 pA/pF.) (*B*) Average normalized $Ca_V2.1$ current (*Left*) and average $Ca_V2.1$ current density (*Right*) as a function of voltage in neurons expressing wt $\alpha_{1A\text{-}2}$ ($n = 8$), RQ ($n = 10$), VA ($n = 5$), or IL ($n = 5$) mutant subunits. For comparison, the normalized I-V curve measured in HEK cells transfected with the same human α_{1A}-subunit (and human $\alpha_{2b}\delta$- and β_{2e}-subunits) is shown as a dotted line. (*C*) Single-channel Ba^{2+} influx of the RQ, VA, and IL mutants relative to that of the wt channel, $(ipo)_{mt}/(ipo)_{wt}$, as a function of voltage, obtained from the current densities in *B*, as described in the text.

of the mutant relative to that of wt, N_{mt}/N_{wt} (Fig. 2*C*). Hans *et al.* (18) obtained $N_{mt}/N_{wt} = 0.37 \pm 0.02$ by counting the number of channels per patch in cell-attached recordings. A lower value ($N_{mt}/N_{wt} = 0.25 \pm 0.06$) was obtained by using Eq. **2** and the data for TM in Fig. 1. The two values were averaged to obtain Fig. 2*C*. With either value, the estimated single-channel Ca^{2+} influx of the TM mutant was much larger than wt over a broad voltage range. Thus, our data support the conclusion that the FHM mutations increase Ca^{2+} influx through single human $Ca_V2.1$ channels.

As mutational changes of functional channel densities in HEK cells may not reflect changes occurring in neurons, we expressed wt and mutant human $Ca_V2.1\alpha_1$ ($\alpha_{1A\text{-}2}$) subunits in cerebellar granule cells in primary culture from $Ca_V2.1\alpha_1^{-/-}$ mice. We have previously shown that these neurons completely lack P/Q Ca^{2+} channels and up-regulate both N- and L-type but not R-type channels, as compared with control (12). The $Ca_V2.1$ current density in transfected neurons was obtained from the amount of whole-cell current inhibited by ω-CTx-MVIIC applied after the specific blocker of N-type channels ω-CgTx-GVIA, as in ref. 12. In neurons expressing the wt human $\alpha_{1A\text{-}2}$-subunit, a maximal $Ca_V2.1$ current density of 24.6 ± 2.4 pA/pF ($n = 32$) was measured at −10 mV (Fig. 3), which is a voltage more than 20 mV more negative than that of the maximal current in HEK cells cotransfected with the same $\alpha_{1A\text{-}2}$-subunit and human $\alpha_{2b}\delta$- and β-subunits, and which is similar to that of the maximal endogenous P/Q current in $Ca_V2.1^{+/+}$ neurons (ref. 12 and Fig. 4, which is published as supporting information on the PNAS web site, www.pnas.org). In neurons expressing mutant human $\alpha_{1A\text{-}2}$-subunits, the $Ca_V2.1$ current density at −10 mV was invariably smaller (Fig. 3*A*). Whereas the reduction of maximal current density in neurons was similar to that measured in HEK cells for the TM, VA, and IL mutants, the reduced maximal current density of the RQ mutant is in striking contrast with the 93% larger density in HEK cells (18).

In neurons expressing mutant human $\alpha_{1A\text{-}2}$-subunits, the voltage dependence of the $Ca_V2.1$ current was invariably shifted

toward hyperpolarized voltages with respect to that in neurons expressing the wt subunit (Fig. 3*B*). As a consequence, the current densities of the mutants were similar to wt at low voltages. Fitting of the normalized I-V curves gave $V_{1/2}$ values of -17.8 ± 1.0 ($n = 8$), -21.9 ± 1.6 ($n = 9$), -29.3 ± 0.8 ($n = 5$) and -31.3 ± 1.9 ($n = 5$) mV for wt, RQ, VA, and IL, respectively. Although the very small P/Q current density of the TM mutant precluded a reliable measurement of a complete I-V curve and an estimation of $V_{1/2}$, its maximal current density was measured at 5 mV more negative voltage than wt (not shown), suggesting activation at lower voltages also for this mutant. The negatively shifted activation of the mutants expressed in granule cells implies that, also in neurons, a common functional effect of FHM mutations is to increase the open probability of $Ca_V2.1$ channels in a broad voltage range. An increased Ca^{2+} influx through single mutant channels in neurons can be inferred from the values of $(ipo)_{mt}/(ipo)_{wt}$ larger than 1, as in Fig. 3*C*. These values were calculated at each voltage from the ratio of the current densities of mutant and wt channels, $I_{mt}/I_{wt,}$ divided by the ratio of the density of channels in the membrane, N_{mt}/N_{wt} (given that $I = Nipo$). If the mutations do not affect the maximal open probability, po_{mx}, N_{mt}/N_{wt} can be obtained from I_{mt}/I_{wt} measured at voltages where $po = po_{mx}$ for mutants with the same unitary conductance as wt and from the same ratio divided by i_{mt}/i_{wt} for mutants with reduced conductance. Considering I_{mt}/I_{wt} at 0 mV (where $po \cong po_{mx}$; see Fig. 5, which is published as supporting information on the PNAS web site), N_{mt}/N_{wt} values of 0.17 ± 0.03, 0.48 ± 0.08, and 0.27 ± 0.03 were obtained for IL, RQ, and VA, respectively. These values are upper limits, and the values of $(ipo)_{mt}/(ipo)_{wt}$ in Fig. 3*C* are lower limits for the RQ and VA mutants if, as found in HEK cells, their po_{mx} is larger than wt, and a fraction of VA mutants has wt conductance (18). The validity of this method for deriving N_{mt}/N_{wt} and ipo_{mt}/ipo_{wt} is supported by the good agreement between the values obtained in HEK cells from whole-cell current densities and from single-channel recordings (see Fig. 5*B*).

The N- and R-type current components were similar in neurons from $Ca_V2.1\alpha_1{}^{-/-}$ mice expressing wt (N-type: 5.4 ± 0.5 pA/pF; R-type: 16.1 ± 1.1 pA/pF, $n = 32$) or mutant human $\alpha_{1A\text{-}2}$-subunits (N-type: 6.0 ± 0.7, 7.4 ± 0.9, 6.5 ± 0.9, 5.1 ± 0.4; R-type: 16.5 ± 1.4, 14.8 ± 1.6, 17.5 ± 1.6, 16.0 ± 1.2 pA/pF, with RQ: $n = 22$, TM: $n = 19$, VA: $n = 14$, and IL: $n = 12$, respectively), and both components were not significantly different from those measured in the same neurons from $Ca_V2.1^{+/+}$ mice (6.1 ± 0.4 and 18.2 ± 1.1 pA/pF, $n = 23$).

Discussion

The findings reported in this article support the following conclusions.

1. FHM mutations increase the Ca^{2+} influx through single human $Ca_V2.1$ channels. A common functional effect of FHM mutations is to shift the activation curve of $Ca_V2.1$ channels to hyperpolarized voltages and thus increase their open probability. This result has two important consequences: (*i*) an increased single-channel Ca^{2+} influx in a large voltage range, despite the reduction in unitary current produced by some mutations; (*ii*) Ca^{2+} influx through mutant channels in response to small depolarizations insufficient to open wt channels. FHM mutants expressed in neurons from $Ca_V2.1\alpha_1{}^{-/-}$ mice or HEK cells showed similar alterations in single-channel function.
2. Another common functional effect of FHM mutations is to decrease the density of functional $Ca_V2.1$ channels and the maximal $Ca_V2.1$ current density in cerebellar granule cells from $Ca_V2.1\alpha_1{}^{-/-}$ mice expressing human $Ca_V2.1\alpha_1$-subunits. Current densities were similar to wt close to the threshold of activation as a consequence of activation at more negative voltages of the mutant channels.
3. The changes in the density of functional channels in the membrane caused by the FHM mutations can be different (even opposite, in the case of RQ) depending on whether the mutant is expressed in a neuron or in an HEK cell. Based on this observation, it cannot be ruled out that changes might be different even among different types of neurons.

The importance of the neuronal environment for studying $Ca_V2.1$ channels is stressed by the striking (>20 mV) difference in the voltage range of activation of human $Ca_V2.1$ channels expressed in neurons or HEK cells. It is unlikely that different auxiliary subunits (mouse vs. human) are responsible for the shift, because only minor changes in channel activation have been measured with different auxiliary subunits in heterologous expression systems (23, 24). Clearly though, some interacting protein and/or biochemical process, present in neurons but not in HEK cells, strongly affects the activation of $Ca_V2.1$ channels.

Our data point to two apparently contradictory functional effects common to all FHM mutations analyzed: an increased Ca^{2+} influx through single $Ca_V2.1$ channels, with relatively small depolarizations ($V < -10$ mV in neurons) but a decreased neuronal $Ca_V2.1$ current density with relatively strong depolarizations ($V > -20$ mV). How can these alterations of $Ca_V2.1$ channel function explain the pathogenesis of FHM and, in particular, lead to its typical episodic neurological symptoms, including aura and headache?

If CSD is the critical event in the pathogenesis of migraine with aura, as indicated by the recent findings of Bolay *et al.* (7) and earlier work, then the alterations in $Ca_V2.1$ channel function induced by FHM mutations should favor the spontaneous occurrence of CSD in the brain of patients. Although the mechanisms for initiation and propagation of CSD are not completely understood, it is clear that an increased neuronal excitability precedes the regenerative depolarization typical of CSD (4). The importance of P/Q type channels in the initiation and spread of CSD has been revealed by Ayata *et al.* (25), who found a striking elevation of the threshold for initiating CSD and a marked reduction in glutamate levels released by K^+-induced depolarization in the neocortex of mouse mutants with spontaneous $Ca_V2.1\alpha_1$ mutations (tg and tg^{la}). Tg^{la} mutants also showed a slower velocity and frequent failure of propagation of CSD and a much larger reduction of excitatory with respect to inhibitory neurotransmitter release. It has been shown that tg and tg^{la} mutations lead to a decreased P/Q current density in both native cerebellar neurons and in heterologous expression systems, and that the tg^{la} mutation shifts the activation curve of $Ca_V2.1$ channels to depolarized voltages and reduces their single-channel open probability (26–28). These data support the conclusion that a reduced Ca^{2+} entry through $Ca_V2.1$ channels reduces neuronal cortical network excitability and makes the cortex more resistant to CSD. It seems unlikely, then, that the functional defect relevant to explain enhanced CSD susceptibility in FHM patients is the reduced neuronal $Ca_V2.1$ current density of FHM mutants. Instead, the functional defect relevant for FHM pathogenesis (or at least its aura phase) could be the increased Ca^{2+} influx through single $Ca_V2.1$ channels that clearly distinguishes the FHM from the tg^{la} mutations. As argued below, this increase could lead to increased local Ca^{2+} influx at presynaptic active zones, despite a global reduction of Ca^{2+} entry in the cell.

Neurotransmitter release at each release site is controlled by a cluster of only a few Ca^{2+} channels located sufficiently close to the Ca^{2+} sensor to contribute to the local Ca^{2+} increase that triggers release in response to single-action potentials (29). $Ca_V2.1$ channels are generally more effective than other Ca^{2+} channel types in triggering release (30–32) as a consequence of

their preferential localization at the release sites (31). Binding of $Ca_V2.1$ channels to syntaxin and synaptosomal-associated protein of 25 kDa contribute to this preferential localization (31, 33). It seems unlikely, then, that the number of $Ca_V2.1$ channels at the release sites would be decreased by FHM mutations in a similar manner as the density of channels in the soma. If a similar number of $Ca_V2.1$ channels are located at the release sites in wt and mutant synapses, the hyperpolarized activation and increased ipo of mutant channels may well lead to an increased action potential-evoked Ca^{2+} influx at the active zones (34) and to a large increase in neurotransmitter release (given the supralinear dependence of release on Ca^{2+} influx and the nonsaturation of the Ca^{2+} sensor during an action potential; ref. 35). If this is the case, and if, as suggested by the data on tg and tg^{la} mice (25, 36), the control of release by $Ca_V2.1$ channels is larger in excitatory than inhibitory synapses, then the FHM mutations are expected to increase neuronal cortical network excitability and make the cortex more susceptible to CSD.

There is some clinical evidence that the migraine aura and the headache are not necessarily sequential, and that the aura may not be the trigger for the pain (37). Functional imaging of patients has provided evidence for a role of the brainstem, particularly the periaqueductal gray (PAG) region, in attacks of migraine without aura (38, 39). Inhibition of P/Q-type channels in PAG has been shown to facilitate trigeminal nociception, thus pointing out a role of these channels in the descending pain-inhibitory system that regulates the perception of pain (40). It is not clear whether the localization of the relevant P/Q channels is presynaptic or postsynaptic, and the mechanism by which their inhibition leads to facilitation (or rather disinhibition) of the second order trigeminal neurons remains unknown. If FHM aura and headache are not sequential but parallel processes, one might even consider the hypothesis that the two apparently contradictory functional effects of FHM mutations may actually underlie the two parallel processes: a decreased $Ca_V2.1$ current density in the PAG may contribute to the headache pathogenesis, whereas an increased Ca^{2+} entry through single $Ca_V2.1$ channels in synaptic terminals in the cortex may underlie the aura.

FHM knock-in mice will allow the testing of these different hypotheses.

We thank Mark Williams (Merck Research Labs, San Diego) for the $\alpha_{1A\text{-}2}$, β_{2e}, and $\alpha_{2b}\delta$ cDNAs. This work was supported by Telethon-Italy (E1297), Ministry of Education, University, Research, Italy (Prin1999), and the Austrian Science Fund (P-14541).

1. Bowyer, S. M., Aurora, K. S., Moran, J. E., Tepley, N. & Welch, K. M. (2001) *Ann. Neurol.* **50,** 582–587.
2. Hadjikhani, N., Sanchez del Rio, M., Wu, O., Schwartz, D., Bakker, D., Fischl, B., Kwong, K. K., Cutrer, F. M., Rosen, B. R., Tootell, R. B. H., *et al*. (2001) *Proc. Natl. Acad. Sci. USA* **98,** 4687–4692.
3. Lauritzen, M. (1996) *Sci. Med.* **3,** 32–41.
4. Somjen, G. G. (2001) *Physiol. Rev.* **81,** 1065–1096.
5. Goadsby, P. J., Lipton, R. B. & Ferrari, M. D. (2002) *N. Engl. J. Med.* **346,** 257–270.
6. Moskowitz, M. A. & Macfarlane, R. (1993) *Cerebrovasc. Brain Metab. Rev.* **5,** 159–277.
7. Bolay, H., Reuter, U., Dunn, A. K., Huang, Z., Boas, D. A. & Moskowitz, M. A. (2002) *Nat. Med.* **8,** 136–142.
8. Ophoff, R. A., Terwindt, G. M., Vergouwe, M. N., van Eijk, R., Oefner, P. J., Hoffman, S. M. G., Lamerdin, J. E., Mohrenweiser, H. W., Bulman, D. E., Ferrari, M., *et al*. (1996) *Cell* **87,** 543–552.
9. Ertel, A. E., Campbell, K. P., Harpold, M. M., Hofmann, F., Mori, Y., Perez-Reyes, E., Schwartz, A., Snutch, T. P., Tanabe, T., Birnbaumer, L., *et al*. (2000) *Neuron* **25,** 533–535.
10. Pietrobon, D. (2002) *Mol. Neurobiol.* **25,** 31–50.
11. Jun, K., Piedras-Renteria, E. S., Smith, S. M., Wheeler, D. B., Lee, S. B., Lee, T. G., Chin, H., Adams, M. E., Scheller, R. H., Tsien, R. W. & Shin, H.-P. (1999) *Proc. Natl. Acad. Sci. USA* **96,** 15245–15250.
12. Fletcher, C. F., Tottene, A., Lennon, V. A., Wilson, S. M., Dubel, S. J., Paylor, R., Hosford, D. A., Tessarollo, L., McEnery, M. W., Pietrobon, D., *et al*. (2001) *FASEB J.* **15,** 1288–1290.
13. Westenbroek, R. E., Sakurai, T., Elliott, E. M., Hell, J. W., Starr, T. V. B., Snutch, T. P. & Catterall, W. A. (1995) *J. Neurosci.* **15,** 6403–6418.
14. Dunlap, K., Luebke, J. I. & Turner, T. J. (1995) *Trends Neurosci.* **18,** 89–98.
15. Sutton, K. G., McRory, J. E., Guthrie, H., Murphy, T. H. & Snutch, T. P. (1999) *Nature (London)* **401,** 800–804.
16. Llinas, R., Sugimori, M., Hillman, D. E. & Cherksey, B. (1992) *Trends Neurosci.* **15,** 351–355.
17. Mori, Y., Wakamori, M., Oda, S., Fletcher, C. F., Sekiguchi, N., Mori, E., Copeland, N. G., Jenkins, N. A., Matsushita, K., Matsuyama, Z. & Imoto, K. (2000) *J. Neurosci.* **20,** 5654–5662.
18. Hans, M., Luvisetto, S., Williams, M. E., Spagnolo, M., Urrutia, A., Tottene, A., Brust, P. F., Johnson, E. C., Harpold, M. M., Stauderman, K. A. & Pietrobon, D. (1999) *J. Neurosci.* **19,** 1610–1619.
19. Kraus, R. L., Sinnegger, M. J., Glossmann, H., Hering, S. & Striessnig, J. (1998) *J. Biol. Chem.* **273,** 5586–5590.
20. Kraus, R. L., Sinnegger, M., Koschak, A., Glossmann, H., Stenirri, S., Carrera, P. & Striessnig, J. (2000) *J. Biol. Chem.* **275,** 9239–9243.
21. Wappl, E., Koschak, A., Poteser, M., Sinnegger, M. J., Walter, D., Eberhart, A., Groschner, K., Glossmann, H., Kraus, R. L., Grabner, M. & Striessnig, J. (2002) *J. Biol. Chem.* **277,** 6960–6966.
22. Xia, Z., Dudek, H., Miranti, C. K. & Greenberg, M. E. (1996) *J. Neurosci.* **16,** 5425–5436.
23. Stea, A., Tomlinson, W. J., Wah Soong, T., Bourinet, E., Dubel, S. J., Vincent, S. R. & Snutch, T. P. (1994) *Proc. Natl. Acad. Sci. USA* **91,** 10576–10580.
24. Hobom, M., Dai, S., Marais, E., Lacinova, L., Hofmann, F. & Klugbauer, N. (2000) *Eur. J. Neurosci.* **12,** 1217–1226.
25. Ayata, C., Shimizu-Sasamata, M., Lo, E. H., Noebels, J. L. & Moskowitz, M. A. (2000) *Neuroscience* **95,** 639–645.
26. Wakamori, M., Yamazaki, K., Matsunodaira, H., Teramoto, T., Tanaka, I., Niidome, T., Sawada, K., Nishizawa, Y., Sekiguchi, N., Mori, E., *et al*. (1998) *J. Biol. Chem.* **273,** 34857–34867.
27. Dove, L. S., Abbott, L. C. & Griffith, W. H. (1998) *J. Neurosci.* **18,** 7687–7699.
28. Lorenzon, N. M., Lutz, C. M., Frankel, W. N. & Beam, K. G. (1998) *J. Neurosci.* **18,** 4482–4489.
29. Meinrenken, C. J., Borst, J. G. & Sakmann, B. (2002) *J. Neurosci.* **22,** 1648–1667.
30. Mintz, I. M., Sabatini, B. L. & Regehr, W. G. (1995) *Neuron* **15,** 675–688.
31. Wu, L. G., Westenbroek, R. E., Borst, J. G. G., Catterall, W. A. & Sakmann, B. (1999) *J. Neurosci.* **19,** 726–736.
32. Qian, J. & Noebels, J. L. (2001) *J. Neurosci.* **21,** 3721–3728.
33. Catterall, W. A. (2000) *Annu. Rev. Cell Dev. Biol.* **16,** 521–555.
34. Borst, J. G. G. & Sakmann, B. (1998) *J. Physiol.* **513,** 149–155.
35. Schneggenburger, R. & Neher, E. (2000) *Nature (London)* **406,** 889–893.
36. Caddick, S. J., Wang, C., Fletcher, C. F., Jenkins, N. A., Copeland, N. G. & Hosford, D. A. (1999) *J. Neurophysiol.* **81,** 2066–2074.
37. Goadsby, P. J. (2001) *Ann. Neurol.* **49,** 4–6.
38. Weiller, C., May, A., Limmroth, V., Juptner, M., Kaube, H., Schayck, R. V., Coenen, H. H. & Diener, H. C. (1995) *Nat. Med.* **1,** 658–660.
39. Bahra, A., Matharu, M. S., Buchel, C., Frackowiak, R. S. & Goadsby, P. J. (2001) *Lancet* **357,** 1016–1017.
40. Knight, Y. E., Bartsch, T., Kaube, H. & Goadsby, P. J. (2002) *J. Neurosci.* **22,** RC213.